NANO LETTERS

2005
Vol. 5, No. 7
1367−1370

Scanning Photocurrent Imaging and Electronic Band Studies in Silicon Nanowire Field Effect Transistors

Yeonghwan Ahn, James Dunning, and Jiwoong Park*

The Rowland Institute at Harvard, Cambridge, Massachusetts 02142

Received April 4, 2005; Revised Manuscript Received June 3, 2005

ABSTRACT

We report optical scanning measurements on photocurrent in individual Si nanowire field effect transistors (SiNW FETs). We observe increases in the conductance of more than 2 orders of magnitude and a large conductance polarization anisotropy of 0.8, making our SiNW FETs a polarization-sensitive, high-resolution light detector. In addition, scanning images of photocurrent at various biases reveal the local energy-band profile especially near the electrode contacts. The magnitude and polarity of the photocurrent vary depending on the gate bias, a behavior that can be explained using band flattening and a Schottky-barrier-type change. This technique is a powerful tool for studying photosensitive nanoscale devices.

Semiconducting nanoscale structures, especially nanowires (NWs)[1] and carbon nanotubes (CNTs),[2,3] offer exciting electronic and optical properties, and have been used recently as core materials in several optoelectronic components. In particular, photoconductance measurements have been performed on InP,[4] ZnO,[5] and GaN[6] NWs as well as CNTs.[7−9] Optical studies on SiNWs, however, have focused primarily on the confinement effects using photoluminescence measurements.[10,11]

In most of the previous studies, the characteristics of individual NW or CNT optoelectronic devices were measured with a wide-field illumination, which lacks the capability to locally probe and measure light-induced responses. Therefore, the spatial profile of the electronic band in individual NWs or CNTs has not been investigated in conjunction with their photoelectronic properties. It is widely known that devices fabricated using semiconducting NWs or CNTs form non-Ohmic contacts and therefore their contact properties play a crucial role in understanding the overall performance.[12−15] Therefore, the development of a local probe technique is highly desirable for investigating how the contact properties and the overall electronic band profile in these devices affect the device characteristics. Recently, scanning photoelectric measurements were demonstrated using CNT devices,[8,9] but the spatial profile of the electronic band in individual NWs has not been investigated in conjunction with their photoelectronic properties.

We report scanning measurements of photoconductance and photocurrents in Si nanowire FETs. We show that Si nanowires can be used as a polarization-sensitive, high-resolution photodetector in the visible range. We also show that the local optoelectronic characteristics provide the detailed spatial information on the energy-band diagram in our SiNW FETs.

Fabrication of SiNW FETs begins with the synthesis of nanowires using the vapor−liquid−solid chemical vapor deposition technique.[16] Au clusters (∼20 nm) were used as a catalyst to grow SiNWs in a flow of SiH_4 and H_2. A small amount of B_2H_4 was sometimes mixed to the flow in order to grow *p*-doped NWs. Both intrinsic and *p*-type NWs were 20−30 nm thick (measured by AFM) and showed a single crystalline structure (confirmed by TEM). SiNWs were then deposited on an oxidized Si wafer substrate with a 220-nm-thick thermal oxide layer that serves as a gate oxide. The conducting back substrate was used as a back gate. Both standard photo- and electron-beam lithography techniques followed by metal evaporation and liftoff were used to define the drain and source electrodes to electrically contact SiNWs. To improve the contact properties, we used a 50-nm-thick Ni layer to contact SiNWs with a rapid thermal annealing process.

The combined optical scanning microscope and transport measurement setup is illustrated in Figure 1a. In this setup, a SiNW device can be illuminated by a diffraction-limited laser spot (diameter ≈ 500 nm) with a wavelength of 532 nm while the device conductance is recorded as a function of the position of the laser spot. The small spot size of the light enables us to record the photoinduced electronic signal that originates from the light illumination at different parts of SiNWs. We can also measure the reflected light simultaneously to decide the absolute position of the laser spot.

In Figure 1b−d, we first show the scanning photoconductance (PC) recorded for a short (∼0.8 μm) *p*-type SiNW

* Corresponding author. E-mail: park@rowland.harvard.edu.

10.1021/nl050631x CCC: $30.25
Published on Web 06/11/2005

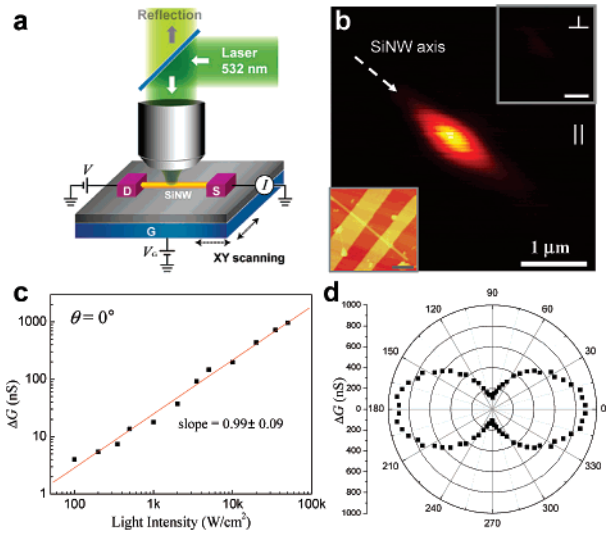

Figure 1. (a) The scanning photocurrent measurement setup. (b) Scanning PC images measured at $V = 0.1$ V with the light polarization parallel (main panel) and perpendicular (upper inset) to the NW. The nanowire PC is represented by the color scale that increases from black (0 nS) through red to yellow (1000 nS). The lower inset shows a topographic AFM image of the device. (1-μm scale bars in the insets) (c) The light instensity and (d) polarization dependence of the SiNW PC with the laser spot at the maximum in the main panel of b. In d, zero corresponds to the parallel polarization. The PC was measured only between zero and 180 degrees and then copied to the other half.

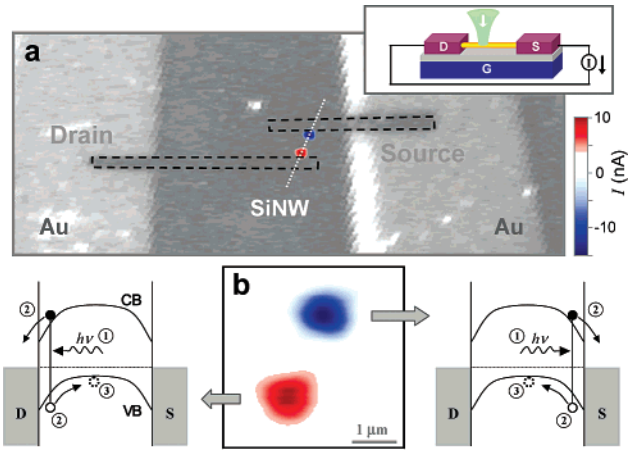

Figure 2. (a) A scanning photocurrent image (color-scale) overlaid on a confocal reflection image (gray-scale) simultaneously taken at $V = V_G = 0$ with a light intensity of 100 kW/cm^2. The image size is 20 by 50 μm. The direction of the positive current is indicated in the upper inset. Red (blue) corresponds to a positive (negative) current. In the reflection image, Ni electrodes (highlighted by dashed lines) are not visible because the light reflection from an Ni surface is weak at 532 nm. (b) An enlarged photocurrent image from part a with energy-band diagrams describing the mechanism of the SPC generation.

device. With the light linearly polarized parallel to the axis of the NW, the device shows a large conductance change only when the light spot is located on the NW (see the main panel, Figure 1b). However, when the light is polarized perpendicular to the NW axis a much smaller PC was observed (upper inset, Figure 1b). Figure 1c shows the PC (denoted by ΔG) as a function of the light intensity (at the maximum conductance change position). The PC increases linearly with the light intensity for more than 2 orders of magnitude with a sensitivity that is similar to that of InP NWs reported previously[4] and significantly larger than that of CNTs.[7] In Figure 1d, we show the polar plot of the PC versus the polarization of the incident light. This clearly shows that the NW conductance is maximum (minimum) when the polarization of the incident light is parallel (perpendicular) to the axis of the NW. The PC anisotropy ratio, $\sigma = (\Delta G_{||} - \Delta G_{\perp})/(\Delta G_{||} + \Delta G_{\perp})$ of this device is 0.8.

These observations prove unambiguously that the SiNW itself is responsible for the photoconductance behavior. It also shows that SiNW devices are excellent polarization-sensitive light detectors with a submicron spatial resolution. The observed PC anisotropy is most likely due to the anisotropy in the light absorption, which is caused by a large dielectric contrast between SiNW ($\epsilon = 11.8$) and its surroundings ($\epsilon \approx 1$). This has been cited previously as the principal mechanism for the photoluminescence and photoconductance polarization anisotropy observed from InP and Si nanowires as well as carbon nanotubes with a wide-field illumination.[4,11]

However, a more intriguing photoelectric behavior was observed when we measured *longer* SiNWs whose length is much larger than the size of the laser spot. In Figure 2a, we overlay two images measured simultaneously. The first image (gray-scale) shows the confocal image of the reflected light measured with the same 532-nm laser. Large gold electrodes are visible in the light gray areas on either side of the SiNW (indicated using a white dotted line based on the AFM topographic image). The second image (color-scale) shows electric current as a function of the laser spot position when $V = 0$. Here, red (blue) indicates a positive (negative) current. A localized positive current spot near the drain electrode as well as a negative current spot near the source electrode is clearly visible in Figure 2a.

These light-induced current "pockets" near the contacts were observed at zero bias from all of the SiNW devices (more than 10 devices) measured to date with magnitudes ranging from 10 to 50 nA for a light intensity of ~100 kW/cm^2 at $V_G = 0$ V. More interestingly, it always shows positive (negative) current with the laser spot close to the drain (source) electrode. The magnitude of the current spot is linearly proportional to the light intensity and shows similar light polarization dependence as in Figure 1d, another behavior that strongly suggests that this localized photocurrent originates from the wire itself.

This striking zero-bias photocurrent behavior can be explained from a simple process shown in Figure 2b. If a SiNW is illuminated near the drain electrode (left diagram), electron−hole pairs will be locally created (1). Then they will be accelerated in opposite directions, that is, electrons to the drain electrode and holes to the middle of the wire driven by the electric field near the electrode contact (2). We draw the electronic bands to be lower near the contacts to match the observed photocurrent polarity (see below). The electrons injected into the drain electrode will contribute to net positive (zero) current when holes are annihilated by

electrons originating from the source (drain) contact (3). As a result, net positive current will flow. The same process will produce a negative current with the light near the source electrode (right diagram), and its polarity will not change as long as the electronic energy is lower near the contacts than in the middle of the nanowire. To our knowledge, this Schottky photocurrent (SPC) behavior, whose current-generating mechanism is similar to that of the Schottky photodiode,[17] has not been studied previously in nanowire devices.[18]

Because the SPC and the electronic band profile are closely related, we can easily deduce the properties of the SiNW electronic band using the behavior of the NW SPC. First, it is clear from the universal presence of the SPC that the electronic band in all of our NW devices is bent near metal contacts. Second, the direction of the bending near the contacts is in the same direction for intrinsic and *p*-doped NWs because the polarity of the SPC is device-independent. In particular, all of the SiNWs in our devices form an accumulation layer at the Ni contacts near zero gate voltage. The magnitude and the polarity of the SPC can be more quantitatively expressed by a simple equation[17]

$$i_{\mathrm{SPC}} = |e|N(P_{\mathrm{D}}^{\mathrm{e}} - P_{\mathrm{D}}^{\mathrm{h}}) = -|e|N(P_{\mathrm{S}}^{\mathrm{e}} - P_{\mathrm{S}}^{\mathrm{h}}) \qquad (1)$$

where N is the number rate of the electron−hole pairs generated by the light and $P_{\mathrm{D(S)}}^{\mathrm{e(h)}}$ is the probability that a photoexcited electron (hole) is transported to the drain (source) electrode. In our experiment, N will vary depending on the light intensity, the light polarization, and the volume of the nanowire under illumination. Also important is the skin depth of Si, which is ~1 μm, at the wavelength of the laser. Based on our experimental conditions, we estimate the maximum value for $|e|N$ to be around 500 nA, which indicates that the conversion efficiency from an absorbed photon to SPC is as large as 10%. This is a large value considering that we ignored the finite extent of the band-bending region and the absorption loss by the metal electrode. A surface treatment such as an antireflection coating would further increase the efficiency.

In Figure 3, we study the gate dependence of the SPC. First, scanning SPC images taken at different gate voltages show a clear polarity switching behavior (see Figure 3a). The white spot (positive SPC) located near the drain at negative gate voltage vanishes in the middle image and then reappears at large positive gate voltages as a black spot (negative SPC). The same behavior is also clearly seen in Figure 3b. The polarity switching of the SPC strongly indicates that the bending direction of the electronic band switches at large gate voltages as illustrated in the band diagrams in the insets. In Figure 3b, we also note that polarity switching of both SPC spots occurs at approximately the same gate bias (marked by an arrow) and the magnitude of the SPC changes almost linearly for a wide gate voltage range (for example, from −10 to 10 V). The latter behavior suggests that the magnitude of the SPC can be used as a local probe for the bending steepness of the electronic band.

From the gate dependence of the SPC together with the DC conductance measurement, we can determine a SiNW electronic band parameter as described below. First, we determine the efficiency of the gate potential $\alpha = |\Delta E/e\Delta V_{\mathrm{G}}|$ (ΔE, the electron band energy change) from the slope of the exponential DC conductance falloff in the subthreshold gate region (inset, Figure 3c).[19] The DC conductance of the NW is measured in the absence of light. Using the measured gate voltages for the *p*-type conductance shut-off (~0 V, arrow in Figure 3c) and the electronic band flattening (~15 V, arrow in Figure 3b) together with $\alpha = 0.037$ and the Si band gap $E_{\mathrm{g}} = 1.12$ eV, we determine the electron barrier height, $\Phi_{\mathrm{Ni}} - \chi$ (see the middle band diagram in Figure 3a), at the Ni/SiNW contact to be 0.57 eV. This is in good agreement with a tabulated value of 0.61 eV for the Ni/Si contact in bulk samples.[17]

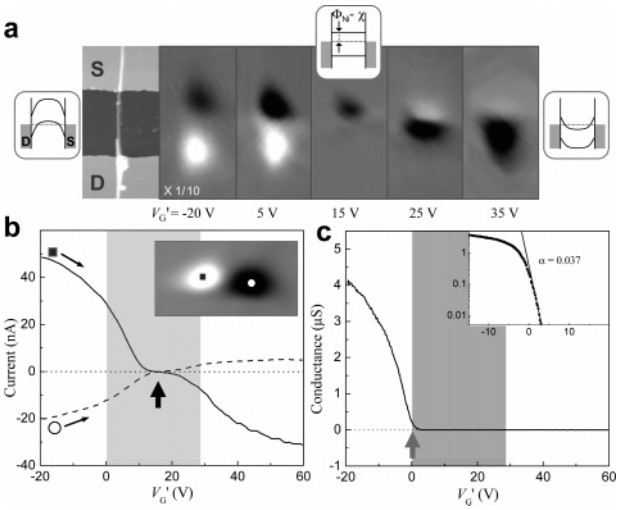

Figure 3. (a) A series of gray-scale (white corresponding to the positive current) scanning SPC images (4 × 2 μm) taken at different gate voltages. An AFM image of the device is shown on the left for comparison. (b) The SPC vs gate voltage. The inset (taken at the zero gate bias) shows the location of the laser spot for each line plot. (c) The DC conductance measured with $V = 10$ mV in the absence of light. The inset shows a semilogarithmic plot of the main panel. This is used to determine the band-gap region, which is represented by the shaded area in b and c. In a−c, the gate axis is corrected for the systematic gate shift caused by the previous gate scans.

Another intriguing observation in Figure 3a is the shrinking distance between the two SPC spots with increasing gate bias. For example, the center-to-center distance is measured at <0.5 μm from the fourth image, which is significantly shorter than that of the first image (~1.5 μm). This behavior contradicts the electrostatic potential calculations, which predict that the band bending, if any, should be strongly confined near the contacts independent of the gate voltage.[12] This unusual behavior is likely caused by the field screening because of various surface and impurity charges near the contacts. This effect has been cited frequently as a cause for several nonideal device characteristics, especially if the devices are not suitably passivated.[20−22] In addition, the n-type DC conductance is completely missing in the device shown here (see Figure 3c), which is consistent with the behavior explained above.

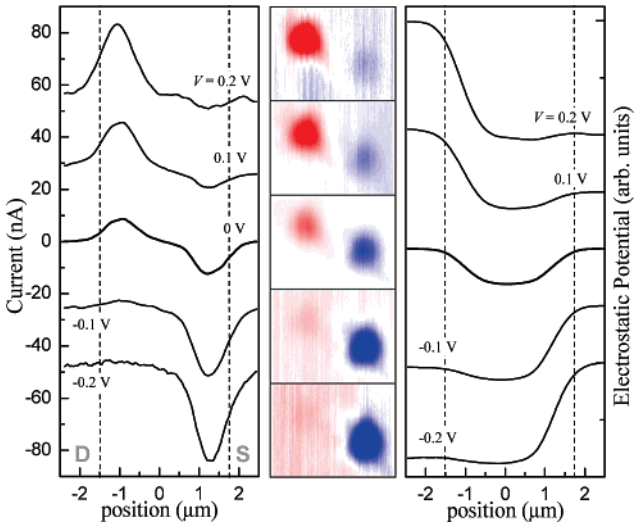

Figure 4. Bias dependence of the SPC. (Middle column) Color-scale scanning photocurrent images (3×4 μm) for different bias voltages. Red (blue) corresponds to the maximum (minimum) current. (Left column) Cross-sectional photocurrent line plots along the NW axis, each offset by 10 nA. (Right column) Electrostatic potential deduced from the left column (offset for clarity).

Finally, we study the bias dependence of the SPC. Surprisingly, we find that the SPC dominates the photoelectric signal for many SiNW devices even when a large bias is applied. Figure 4 shows the scanning photocurrent images (middle column) measured at different bias voltages (from 0.2 V to −0.2 V, top to bottom) for the same device as that in Figure 2. The SPC spots are clearly visible with their circular shape and the center position roughly the same at all biases. However, the intensity of the positive (negative) SPC spot becomes weaker at negative (positive) biases, finally vanishing near −0.2 V (0.2 V). Also notable is the fact that no significant photoinduced current is observed when the light is focused on the middle of the NW. These behaviors are most likely due to a large potential drop near the contacts as well as a relatively flat band in the middle of the SiNW.

In fact, our scanning SPC measurement, especially its polarity, can be used to probe the behavior of the local electrostatic potential, especially its ups and downs. It is also likely that the intensity of the SPC will be roughly proportional to the local electric field (equivalently the steepness of the potential) as discussed earlier. Therefore, the spatial map of the electrostatic potential profile can be captured qualitatively by integrating the SPC line scans shown on the left side. The electrostatic potential profile calculated this way is shown along the NW axis in the right column. We can clearly see in which direction the potential is bent and also where it becomes level.

In conclusion, we have measured the photoconductance and photocurrent in individual SiNW FETs using the combined optical scanning microscope and transport measurement setup. We observe a surprisingly strong photocurrent near the contacts, which originates from the electronic band bending. The behavior of this photocurrent was investigated at different gate and drain-source biases, revealing its potential application as a scanning probe for the electronic band structure within the nanowire. This unique photoelectric phenomenon could also be used to fabricate a highly sensitive point photodetector, which could find applications for high-resolution position sensors, a local biosensor for optically active species, and advanced photosensitive scanning probe tips.

Acknowledgment. We thank C. M. Lieber, B. Timko, W. Hill, and C. Stokes for their help in setting up the nanowire growth setup. We also thank M. Burns and P. Fischer for helpful discussions. This work was fully supported by the Rowland Junior Fellowship program.

References

(1) Lieber, C. M. *MRS Bull.* **2003**, *28*, 486.
(2) McEuen, P. L.; Park, J. Y. *MRS Bull.* **2004**, *29*, 272.
(3) Avouris, P. *MRS Bull.* **2004**, *29*, 403.
(4) Wang, J. F.; Gudiksen, M. S.; Duan, X. F.; Cui, Y.; Lieber, C. M. *Science* **2001**, *293*, 1455.
(5) Kind, H.; Yan, H. Q.; Messer, B.; Law, M.; Yang, P. D. *Adv. Mater.* **2002**, *14*, 158.
(6) Han, S.; Jin, W.; Zhang, D. H.; Tang, T.; Li, C.; Liu, X. L.; Liu, Z. Q.; Lei, B.; Zhou, C. W. *Chem. Phys. Lett.* **2004**, *389*, 176.
(7) Freitag, M.; Martin, Y.; Misewich, J. A.; Martel, R.; Avouris, P. H. *Nano Lett.* **2003**, *3*, 1067.
(8) Balasubramanian, K.; Fan, Y. W.; Burghard, M.; Kern, K.; Friedrich, M.; Wannek, U.; Mews, A. *Appl. Phys. Lett.* **2004**, *84*, 2400.
(9) Balasubramanian, K.; Burghard, M.; Kern, K.; Scolari, M.; Mews, A. *Nano Lett.* **2005**, *5*, 507.
(10) Bai, Z. G.; Yu, D. P.; Wang, J. J.; Zou, Y. H.; Qian, W.; Fu, J. S.; Feng, S. Q.; Xu, J.; You, L. P. *Mater. Sci. Eng. B* **2000**, *72*, 117.
(11) Qi, J. F.; Belcher, A. M.; White, J. M. *Appl. Phys. Lett.* **2003**, *82*, 2616.
(12) Heinze, S.; Tersoff, J.; Martel, R.; Derycke, V.; Appenzeller, J.; Avouris, P. *Phys. Rev. Lett.* **2002**, *89*, 106801.
(13) Appenzeller, J.; Knoch, J.; Derycke, V.; Martel, R.; Wind, S.; Avouris, P. *Phys. Rev. Lett.* **2002**, *89*, 126801.
(14) Javey, A.; Guo, J.; Paulsson, M.; Wang, Q.; Mann, D.; Lundstrom, M.; Dai, H. J. *Phys. Rev. Lett.* **2004**, *92*, 106804.
(15) Yaish, Y.; Park, J. Y.; Rosenblatt, S.; Sazonova, V.; Brink, M.; McEuen, P. L. *Phys. Rev. Lett.* **2004**, *92*, 046401.
(16) Cui, Y.; Lauhon, L. J.; Gudiksen, M. S.; Wang, J. F.; Lieber, C. M. *Appl. Phys. Lett.* **2001**, *78*, 2214.
(17) Sze, S. M., *Physics of Semiconductor Devices*, 2nd ed.; John Wiley & Sons: New York, 1981.
(18) The thermal effect in our devices will be negligible as explained below. The upper limit of the temperature increase caused by the laser illumination on SiNWs can be estimated based on the Si thermal resistivity (0.76 K·cm/W at 300 K) and the device geometry, assuming that all of the absorbed photons are converted to heat. The estimated value is less than 2 K when the light with an intensity of 100 kW/cm^2 illuminated the middle of a SiNW (where heat dissipation is the slowest) and if there is no heat dissipation through the silicon oxide substrate. The thermoelectric potential will be around 1 mV in this case, which can create a thermoelectric current as much as a few nA. This is smaller by 1 order of magnitude than the typical SPC measured from our devices. Furthermore, the actual temperature increase will be much smaller if the light is located near the contact where heat dissipation is faster and if we allow heat dissipation through the substrate. In addition, not all of the photon energy will be converted to heat in real devices.
(19) Rosenblatt, S.; Yaish, Y.; Park, J.; Gore, J.; Sazonova, V.; McEuen, P. L. *Nano Lett.* **2002**, *2*, 869.
(20) Cui, Y.; Zhong, Z. H.; Wang, D. L.; Wang, W. U.; Lieber, C. M. *Nano Lett.* **2003**, *3*, 149.
(21) Kim, W.; Javey, A.; Vermesh, O.; Wang, O.; Li, Y. M.; Dai, H. J. *Nano Lett.* **2003**, *3*, 193.
(22) Neudeck, G. W.; Pierret, R. F. *Field Effect Devices*; Addison-Wesley Publishing Company: Reading, MA, 1990.

NL050631X